Plant, Cell and Environment (2005) **28**, 633–641

Dynamics of stomatal patches for a single surface of *Xanthium strumarium* L. leaves observed with fluorescence and thermal images

JEVIN D. WEST[1], DAVID PEAK[2], JAMES Q. PETERSON[3] & KEITH A. MOTT[1]

[1]*Biology Department, Utah State University, Logan, UT 84322–5305, USA* [2]*Physics Department, Utah State University, Logan, UT 84322–4415, USA and* [3]*Space Dynamics Laboratory, Utah State University, Logan UT 84322–9700, USA*

ABSTRACT

Fluorescence and thermal imaging were used to examine the dynamics of stomatal patches for a single surface of *Xanthium strumarium* L. leaves following a decrease in ambient humidity. Patches were not observed in all experiments, and in many experiments the patches were short-lived. In some experiments, however, patches persisted for many hours and showed complex temporal and spatial patterns. Rapidly sampled fluorescence images showed that the measurable variations of these patches were sufficiently slow to be captured by fluorescence images taken at 3-min intervals using a saturating flash of light. Stomatal patchiness with saturating flashes of light was not demonstrably different from that without saturating flashes of light, suggesting that the regular flashes of light did not directly cause the phenomenon. Comparison of simultaneous fluorescence and thermal images showed that the fluorescence patterns were largely the result of stomatal conductance patterns, and both thermal and fluorescence images showed patches of stomatal conductance that propagated coherently across the leaf surface. These nondispersing patches often crossed a given region of the leaf repeatedly at regular intervals, resulting in oscillations in stomatal conductance for that region. The existence of these coherently propagating structures has implications for the mechanisms that cause patchy stomatal behaviour as well as for the physiological ramifications of this phenomenon.

Key-words: chlorophyll fluorescence; patchy; stomata; stomatal conductance; thermal imaging.

INTRODUCTION

Stomatal responses to environmental stimuli are sometimes markedly heterogeneous (for reviews see Terashima 1992; Beyschlag & Eckstein 1998; Mott & Buckley 1998, 2000). Even under apparently uniform environmental conditions, groups of dozens to thousands of stomata can behave differently from stomata in adjacent areas. When this occurs, the result is a patchy distribution of stomatal conductance across the leaf surface, which can have important implications for the interpretation of gas-exchange measurements (Terashima *et al*. 1988; Meyer & Genty 1998; Buckley, Farquhar & Mott 1999), and poses problems in scaling guard cell processes to leaf level stomatal conductance (Buckley, Farquhar & Mott 1997). Patchy stomatal conductance is not detectable with gas-exchange measurements, so it has been studied with techniques such as starch staining (Terashima *et al*. 1988), pressure infiltration (Beyschlag & Pfanz 1992) and autoradiography (Wise, Ortiz-Lopez & Ort 1992). These techniques are destructive and therefore of limited use in studying the *dynamics* of stomatal patches.

Imaging of chlorophyll fluorescence provides a non-destructive technique for determining the spatial distribution of photosynthesis. If there are no changes in intrinsic photosynthetic capacity, then such images can also be interpreted in terms of stomatal conductance distributions (Daley *et al*. 1989; Meyer & Genty 1998).

Several studies have documented complex temporal and spatial patterns of chlorophyll fluorescence in response to environmental stimuli (Cardon, Mott & Berry 1994; Siebke & Weis 1995). Fluorescence patches have been found to be stable, oscillatory, or exhibit unpredictable changes in both space and time, and most of this behaviour has been attributed to patchy stomatal conductance. These findings have raised questions about the effect of stomatal patchiness on gas-exchange optimality and the possible physiological roles of stomatal patchiness. In addition, the underlying mechanisms for the formation and dynamics of stomatal patches remain uncertain. It has been proposed that hydraulic interactions in the epidermis might serve to coordinate movements of stomata within a patch (Mott, Denne & Powell 1997; Mott, Shope & Buckley 1999; Mott & Franks 2001). Computer simulations show that these hydraulic interactions can produce heterogeneous stomatal conductance (Haefner, Buckley & Mott 1997), but the simulations lack many aspects of the patch structure and dynamics seen in leaves.

Correspondence: Keith Mott. E-mail:kmott@biology.usu.edu

Thermography provides another non-destructive technique for studying patchy stomatal conductance. Interpretation of thermal images in terms of stomatal conductance depends on the fact that leaf temperature is a function of transpiration and therefore a function of stomatal conductance. There have been fewer studies using thermography to quantify patchy stomatal conductance, presumably because the equipment is more expensive and less common than that required for chlorophyll fluorescence. However, leaf temperature has enough spatial resolution to yield information on the variability of stomatal conductance across a leaf surface (Jones 1999).

A major limitation to developing hypotheses for the mechanisms of the patch dynamics seen in leaves is the lack of detailed time-course data that unequivocally represent stomatal patchiness. Existing data for fluorescence images are deficient for this purpose in four ways. First, in previous studies (Cardon *et al*. 1994; Siebke & Weis 1995), images were taken at intervals of several minutes, yet these studies found that many changes in fluorescence occurred on a shorter time scale. This raises the question of whether aspects of patch dynamics were missed in these relatively under-sampled time courses. Second, some of the data are complicated by the fact that the pattern of stomatal patches can be different for the two surfaces of an amphistomatous leaf (Mott, Cardon & Berry 1993). This is a problem because in a thin amphistomatous leaf, the supply of CO_2 to the mesophyll depends on diffusion through both surfaces (Mott & O'Leary 1983; Parkhurst *et al*. 1986; Mott 1988; Parkhurst & Mott 1990). Patterns of chlorophyll fluorescence will therefore reflect the sum of the conductances of the two surfaces. It seems possible that at least some of the complexity of patch behaviour observed in amphistomatous leaves arises from this effect. Third, the use of a short high-intensity flash of light in capturing some types of fluorescence images might plausibly affect (or even cause) the observed pattern of stomatal conductance patches. Finally, studies have shown that fluorescence patches can sometimes be at least partially caused by changes in intrinsic photosynthetic capacity, which calls into question whether the observed patterns of fluorescence are representative of stomatal patterns.

The purpose of this study was to characterize the temporal and spatial dynamics of stomatal patchiness, addressing the four points discussed above. We addressed the problem of undersampling by acquiring fluorescence images every 20 s. We examined patch dynamics for a single leaf surface by providing CO_2 to only one surface of an amphistomatous leaf. We investigated the effect of regularly spaced high intensity flashes of light on patch dynamics by acquiring fluorescence images without the flashes, and comparing the dynamics in the images to those acquired with the flashes. Finally, to verify that the observed patterns of chlorophyll fluorescence were caused by stomatal conductance patterns, we employed another non-destructive method for observing spatial and temporal patterns of stomatal conductance over a leaf surface: infrared imaging (thermography) (Jones 1999).

MATERIALS AND METHODS

Plant material

Cocklebur (*Xanthium strumarium* L.) plants were grown in 1.0 L pots containing a soil-less medium consisting of peat, perlite and vermiculite (1 : 1 : 1, by vol.). Plants were grown in a controlled environment greenhouse with day and night temperatures of 30 and 20 °C, respectively. When necessary, day length was extended to 16 h with high-pressure sodium lamps that provided a photon flux density (PFD) of approximately 1000 μmole m^{-2} s^{-1} at the top of the plants. Pots were watered to excess daily with a dilute nutrient solution containing 9.1 mM N, 1.8 mM P, 2.7 mM K, and 11 μM chelated Fe (Peter's 20-10-20; Grace Sierra Horticultural Products Co., Milpitas, CA, USA). Plants used for experiments were at least 6 weeks old, and the leaves chosen for use were fully mature but not senescing.

Gas-exchange measurements

Gas-exchange measurements were made with a standard open system that has been described previously (Mott 1988). Briefly, the system employed mass-flow controllers to precisely mix CO_2, O_2, N_2, and H_2O vapour in the gas supplied to the leaf chamber. The absolute concentration of CO_2 in the gas stream was measured using an infra-red gas analyser (model MKIII; Analytical Development Co, Hoddesdon, Herts., UK), and the absolute concentration of H_2O in the gas stream was determined with a dewpoint hygrometer (Dew-10; General Eastern, Watertown, MA, USA). Differences in CO_2 and H_2O concentrations in the gas streams before and after the chamber were determined using an infrared gas analyser (Model 6262; Li-Cor Inc., Lincoln, NE, USA). Measurements were made using two different chambers. The first chamber (chamber 1) enclosed a square area (2.54 cm × 2.54 cm) of the leaf and the gas in the chamber was stirred with three miniature fans creating a boundary layer conductance for each surface of 3.33 mol m^{-2} s^{-1}. For experiments involving thermal imaging, a circular chamber (diameter = 2.54 cm) with a clear top made of calcium fluoride (thickness = 0.5 cm) was used. This material was transparent in the 2.5–3.5 μm range used by the thermal camera. In this chamber (chamber 2), stirring was created from the inflow of the gas, and the boundary layer conductance was 1.5 mol m^{-2} s^{-1}. Major veins were avoided when placing the chambers on a leaf. In all cases, light was provided by a 300-W Xenon lamp (ILC Technology, Sunnyvale, CA, USA), filtered to remove wavelengths above 700 nm and delivered to the leaf with a liquid light guide. The PFD between 400 and 700 nm incident on the leaf was approximately 1000 μmol m^{-2} s^{-1}. For each experiment, the leaf was allowed to reach steady state at an O_2 concentration of 20 mmol mol^{-1}, an H_2O vapour concentration of 24 mmol mol^{-1} and a leaf temperature of 25 °C. This created a Δw for the leaf of approximately 12 mmol mol^{-1}. The CO_2 concentration for the upper surface was maintained at 350 ± 5 μmol mol^{-1}, while that for the lower sur-

face was reduced until there was no CO_2 exchange across the lower surface. The concentration for the lower surface varied among leaves and during the experiments, but it was approximately 125 μmol mol^{-1}, and it was approximately 10–20 μmol mol^{-1} less than the calculated intercellular CO_2 concentration for the upper surface. H_2O vapour concentration was lowered to 14 mmol mol^{-1} for the upper surface to initiate patchy stomatal conductance on that surface.

Thermal and chlorophyll fluorescence imaging

Images of chlorophyll fluorescence for the leaf area in both chambers were acquired with a peltier-cooled CCD camera (Coolsnap HQ; Roper Scientific, Photometrics, Tucson, AZ, USA), which provided 8-bit greyscale images that were 512 pixels × 512 pixels in size. The camera was fitted with a 18–108 mm zoom lens and a 700-nm high pass filter. Images of fluorescence at the actinic light level (F′ images) were taken every 20 s in all experiments. In some experiments, images were also taken every 180 s during a 1-s flash of light at a PFD of 4000 μmol m^{-2} s^{-1} (F_m' images). F_m' images were acquired using an exposure time that was 25% of that for the F' images. Thus, fluorescence yield per absorbed photon was comparable for the two types of images. Images representing $1 - F'/F_m'$ were created using pixel-by-pixel division of the images, and the resulting pixel values were scaled between 0 and 255. To make these images more visually comparable to the thermal images (i.e. so that areas of high conductance were dark), the greyscale values were inverted by subtracting each pixel intensity value from 255.

Thermal images of the leaf area in chamber 2 were obtained using a cryogenically cooled, midwave, infrared imaging camera (Model SBF125; Santa Barbara Focalplane, Santa Barbara, CA, USA) that was fitted with a 2.5–3.5 μm bandpass filter and a 50-mm F2.3 germanium lens. The camera had a noise-equivalent ΔT of 0.01 K. Eight-bit greyscale images containing 320 pixels × 256 pixels were acquired every 20 s. The camera was calibrated at 20 and 30 °C for each experiment using a Peltier-controlled blackbody calibration source (model SR-80; CI Systems, Inc, Westlake Village, CA, USA). The spread of 256 greyscales over a 10 K range provided a thermal resolution of 0.04 K. The emissivity of the leaf was assumed to be 1.0.

To compare thermal and fluorescence patterns for the leaf area in chamber 2, it was necessary to image the leaf with both cameras simultaneously, which meant that the images could not be taken from exactly the same angle. The slightly different angles for the two cameras made it difficult to exactly identify the same area of the leaf in the two types of images. This problem was exacerbated by the fact that the images had different pixel densities. Equivalent regions of the leaf in the two image types were identified by establishing a known reference point (i.e. the intersection of two major veins) as an origin and mapping the pixels in the two images by their horizontal and vertical distance from that origin. This was done using image processing software (Image Pro Plus, Media Cybernetics, Inc., Silver Spring, MD, USA) and did not involve distortion of each image.

Correlation analysis

To show quantitatively that the dynamic patterns of chlorophyll fluorescence and leaf temperature were similar, a correlation analysis was performed. Pixel intensity was averaged over an area of approximately 2.3 mm × 2.3 mm for equivalent regions of both fluorescence and thermal images. This area contained approximately 800 stomata on the upper surface. The resolution of the images was slightly different for each experiment because of differences in camera position, but on average this area was 21 pixels × 21 pixels in the thermal images, and 43 pixels × 43 pixels in the fluoresence images. This area contained sufficient pixels so that random noise at the pixel level was largely eliminated, but it was small enough to capture the dynamics of a single patch. Twenty of these areas were chosen, avoiding major veins, and average pixel intensities were calculated for approximately 1000 images in a time series. The Pearson cross-correlation coefficient was then calculated for the average pixel intensity of the boxed regions of the fluorescence images and the thermal images.

RESULTS

To begin each experiment, a leaf was brought to steady state with $\Delta w = 10$ mmol mol^{-1} for both surfaces but with CO_2 supplied only through the upper surface as described in Methods and Materials. Fluorescence images, both F' and $1 - F'/F_m'$, and thermal images of leaves under these conditions were essentially homogeneous.

To initiate stomatal patchiness, Δw for the upper surface was raised to 22 mmol mol^{-1}, but maintained at 12 mmol mol^{-1} for the lower surface. Following this treatment, stomatal conductance for the upper surface (as measured by gas exchange) declined, whereas that for the lower surface remained approximately constant. The dynamics of the decline in conductance for the upper surface varied from experiment-to-experiment despite attempts to exactly replicate the experimental conditions. We performed 43 experiments with fluorescence imaging, using chamber 1. In 28 of these experiments, stomatal conductance declined over a period of 20–40 min and then became stable at a lower value. In 13 of these 28 experiments, fluorescence images were briefly heterogeneous as conductance declined but became homogeneous when conductance became stable. In the other 15 of these 28 experiments, however, conductance took longer than 40 min to become stable and fluorescence heterogeneity persisted. The duration of instability varied among experiments, and during these extended periods of fluorescence heterogeneity, we were able to capture long sequences of fluorescence images. Some of these sequences showed remarkable dynamics. Two time-lapse movies (WebMovie1.avi and WebMovie2.avi) of these dynamics (one of F' images and one of $1 - F'/F_m'$ images) are available at the journal's website

(http://www.blackwellpublishing.com/pce). Both movies represent 6 h of data compressed into about 15 s.

To test whether the remarkable heterogeneity in fluorescence observed in the above experiments was representative of heterogeneity in stomatal conductance rather than in some other aspect of the photosynthetic machinery, we conducted six experiments in which fluorescence and thermal images were captured simultaneously. In four of the six experiments, fluorescence and thermal images were spatially uniform or showed only short-lived patches. In the other two experiments, dynamic patches in the fluorescence and thermal images developed approximately 20 min after the change in Δw and persisted for several hours. In both of these experiments, thermal images and F' images were acquired every 20 s to be sure that all stomatal dynamics were captured. In one experiment, F_m' images were also acquired every 3 min for calculation of $1 - F'/F_m'$ images. This was done to examine the possible effect of the high-intensity flashes of light, necessary to obtain F_m' images, on stomatal dynamics

To verify that there was no cross sensitivity between the fluorescence camera and the thermal camera, we perturbed fluorescence independently of leaf temperature by lowering ambient CO_2 (c_a) for the upper surface from 350 to 0 μmol mol^{-1} in a step change. We then captured fluorescence and thermal images of the leaf 30 s after the change in $[CO_2]$. This period of time was too short for stomata to respond, but long enough for the decreased availability of CO_2 to influence chlorophyll fluorescence. These images showed a two-fold increase in chlorophyll fluorescence but no change in leaf temperature (Fig. 1). Thermocouple measurements of leaf temperature also showed no effect of this treatment on leaf temperature. To change leaf temperature independently of chlorophyll fluorescence we increased the Δw for the leaf from 12 to 22 mmol mol^{-1} and captured fluorescence and thermal images 30 s after the change in Δw. This period of time was too short for stomata to respond, but long enough for the increased rate of evaporation to affect leaf temperature. Thermal images showed a decrease in pixel intensity (Fig. 2) corresponding to a decrease in the average leaf temperature from 24.7 to 23.6 °C. This agreed well with leaf temperature as measured by the thermocouple, which decreased from 25.0 to 23.9 °C. Fluorescence intensity, however, was unaffected by this treatment (Fig. 2).

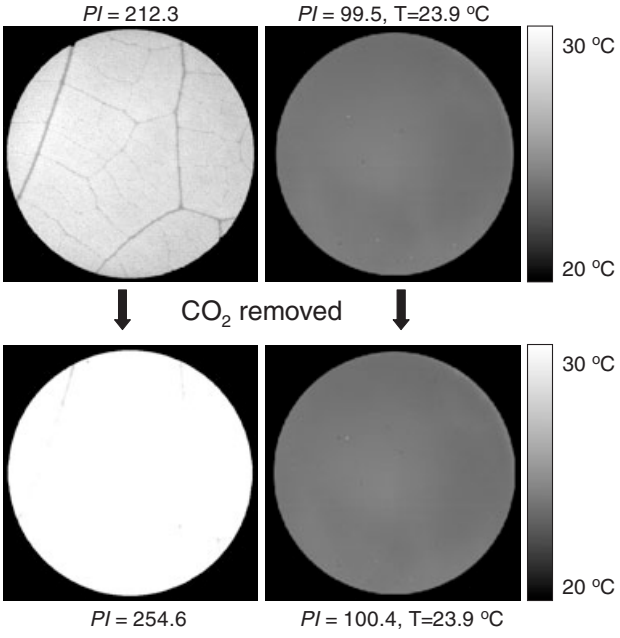

Figure 1. Simultaneous fluorescence (F') and thermal images before, and 30 s after, lowering ambient CO_2 (c_a) for the upper surface from 350 to 0 μmol mol^{-1}. The left and right columns are fluorescence and thermal images, respectively. PI represents the average pixel intensity for the images. These images showed a two-fold increase in PI for the chlorophyll fluorescence images but essentially no change in PI for the thermal images. Thermocouple measurements of leaf temperature also showed no effect of this treatment on leaf temperature.

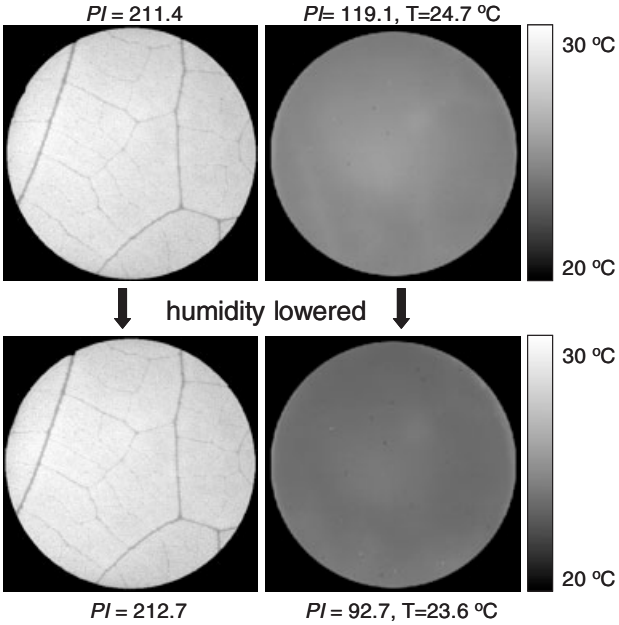

Figure 2. Simultaneous fluorescence (F') and thermal images before, and 30 s after, increasing Δw from 12 to 22 mmol mol^{-1}. The left and right columns are fluorescence and thermal images, respectively. PI represents the average pixel intensity for the images. For the fluorescence images, PI remained essentially unchanged after the humidity perturbation. The thermal images, however, showed a decrease in PI, corresponding to a decrease in the average leaf temperature from 24.7 to 23.6 °C. This agreed well with the thermocouple measurements, which decreased from 25.0 to 23.9 °C.

Sequences of fluorescence and thermal images were compared with one another to determine if there were differences in the spatial and temporal patterns of the patches. The first type of comparison made was visual. Fluorescence and thermal images taken at the same time were displayed side by side and compared. Figure 3 shows F', $1 - F'/F_m'$,

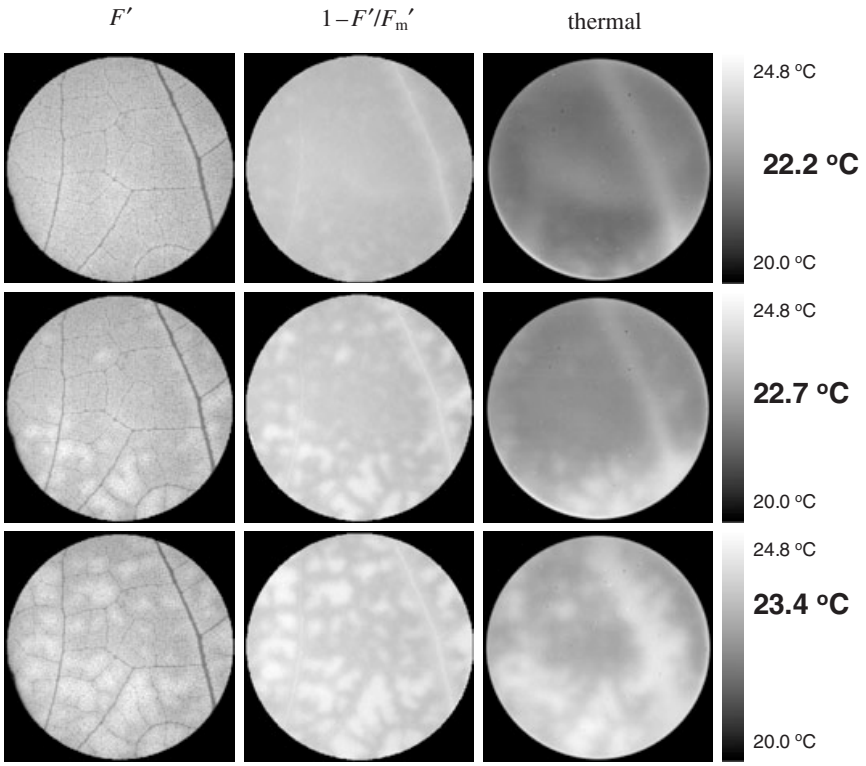

Figure 3. Simultaneous F', $1 - F'/F_m'$, and thermal images (columns, left to right) for three time points during one experiment. (Greyscale pixel values were inverted for $1 - F'/F_m'$ images to make them easier to compare to thermal images.) The temperature scale to the right of the thermal images was scaled for the 255 grey-scale thermal images between 20.0 and 24.8 °C. The bold numbers to the right of the scale are the average temperatures calculated from each thermal image. Images were taken at 5, 30 and 180 min after Δw was increased for the upper surface. The circular leaf area shown has a diameter of 2.54 cm, which includes approximately 100 000 stomata.

and thermal images for three time points during the experiment shown in WebMovie4.avi. Although the fluorescence and thermal images are clearly not identical, the similarity between the two images at any time is striking. This similarity is better shown by the time-lapse movies of thermal and fluorescence images side-by-side (WebMovie3.avi and WebMovie4.avi, available at http://www.blackwellpublishing.com/pce). In both movies, 3 s represents approximately 1 h of data. The thermal and fluorescence movies were acquired separately and then sized similarly so that they could be placed side by side for comparison.

Comparison of F' images with $1 - F'/F_m'$ images reveals that in the experiments reported in this study, most of the heterogeneity in fluorescence was contained within the F′ images (Fig. 3, compare left two columns). To quantify the similarities among thermal, F' and $1 - F'/F_m'$ images, we

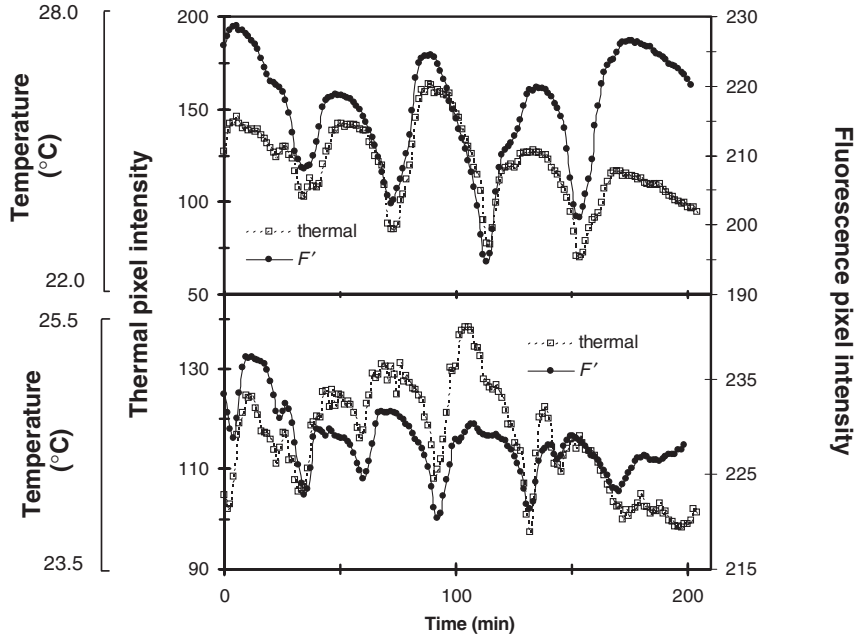

Figure 4. Average pixel intensity versus time for 2.3 mm × 2.3 mm regions of F' and thermal images. The temperatures corresponding to the thermal pixel values are given by the outside left axis. The two panels show different regions from the same experiment, and the complete dataset is shown in WebMovie3.avi (web only data). The regions were selected based on the richness of their dynamics. The Pearson correlation coefficients between F' and thermal pixel intensity were 0.775 and 0.756 for the top and bottom panel, respectively. Both values are significant at $P < 0.01$.

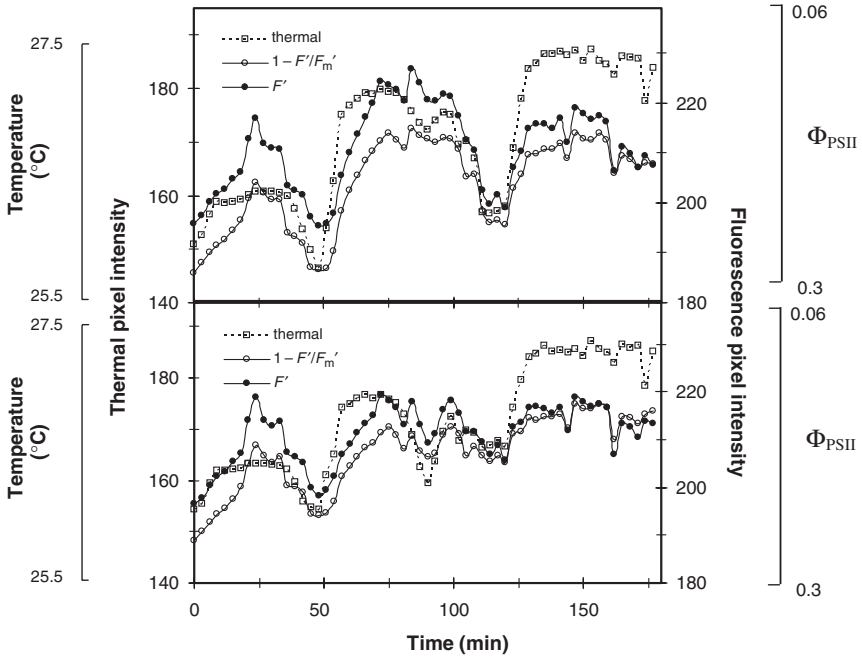

Figure 5. Average pixel intensity versus time for 2.3 mm × 2.3 mm regions of F', 1 – F'/F_m', and thermal images. The temperature corresponding to the thermal pixel value is given by the outside left axis, and the Φ_{PSII} value corresponding to the 1 – F'/F_m' pixel value is given by the outside right axis. The two panels show different regions from the same experiment. The regions were based on the richness of their dynamics. The Pearson correlation coefficients between F_m' and 1 – F'/F_m' data were 0.860 and 0.859 for the top and bottom panels, respectively. For F_m' and thermal data, they were 0.728 and 0.685 for the top and bottom panels, respectively. For 1 – F'/F_m' and thermal data, the coefficients were 0.892 and 0.917 for the top and bottom panels, respectively. All correlations were significant at $P < 0.01$.

plotted the average pixel intensity of 20 of the 2.3 mm × 2.3 mm regions against time for all three types of images. Many of these areas had low activity in both thermal and fluorescence images, but Fig. 4 shows data for four areas with high activity. Figure 4 shows data for an experiment in which only F' images were captured, and Fig. 5 shows data from an experiment in which 1 – F'/F_m' images were calculated. Pixel intensities of F_m', 1 – F'/F_m' and thermal images were highly correlated, as indicated by the correlation coefficients given in the captions.

Although the behaviour of stomatal conductance patches was highly unpredictable, some areas exhibited repetitive behaviour (see Figs 4 & 5). In many cases, however, close examination of time-lapse movies showed that this repetitive behaviour was the result of circulating movement of coherent patches across the leaf. The movement of these fluorescence patches can be seen clearly in the time-lapse movies (WebMovies 1–4), but it is difficult to discern from still images. In an attempt to capture these dynamics in still images, we created difference images in which pixels that increase in intensity over a period of 1 min are shown as red, and pixels that decrease are shown as yellow. Pixels that do not change are black. Figure 6 shows a series of these difference images, calculated from 1 – F'/F_m' and thermal data, in which a region of increasing pixel intensity moves upwards in three images 40 s apart.

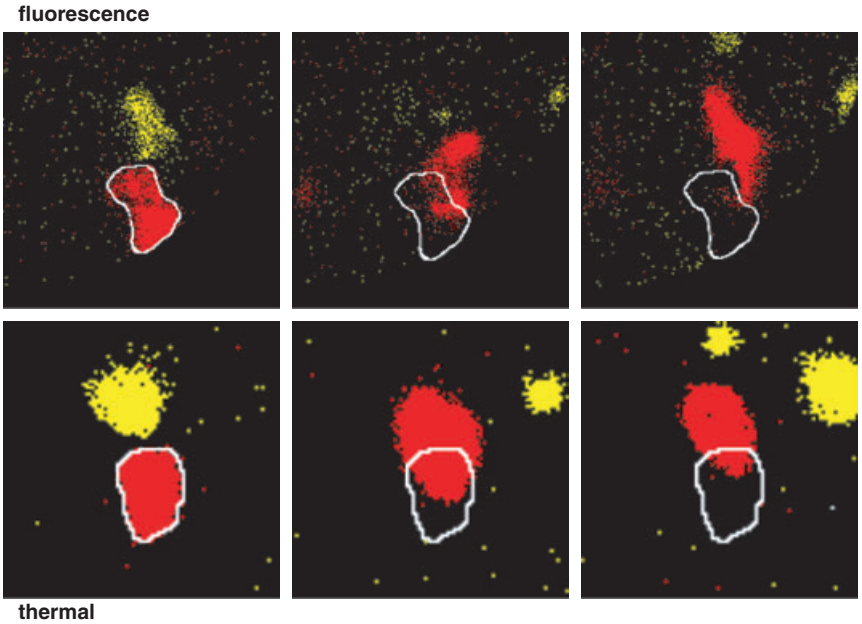

Figure 6. Coherent movement of stomatal conductance patches. Fluorescence (top row) and thermal (bottom row) images were coloured according to stomatal conductance trends. To produce the images shown, images 1 min apart were compared. If the pixel intensity increased by more than 10 units over this time, it was coloured red. If it decreased by more than 10 units, it was coloured yellow. If the pixel changed less than 10 units, it was coloured black. The three images shown are 40 s apart, and the area shown in the figure is approximately 0.49 cm^2. The tracing shows the movement of the red patch, which contained approximately 2000 stomata and moved at approximately 20 $\mu m\ s^{-1}$.

DISCUSSION

In this study, we visualized stomatal patchiness for a single surface of *Xanthium strumarium* leaves using images of chlorophyll fluorescence. Although *Xanthium* is amphistomatous, its leaves are sufficiently thin and porous that CO_2 can be supplied to the entire mesophyll from only one surface (Mott & O'Leary 1983; Parkhurst *et al*. 1986; Mott 1988; Parkhurst & Mott 1990). In this study, c_i values were lower than would typically be reported for C_3 leaves. This was caused by two factors: the low O_2 concentrations, which produced a high photosynthetic rate without a concomitant increase in stomata conductance, and the fact that CO_2 was supplied only through the upper surface. Our results using this technique are similar to previous studies using similar methods (Mott & O'Leary 1983; Parkhurst *et al*. 1986; Mott 1988; Parkhurst & Mott 1990), and we conclude that in our experiments, photosynthesis, and therefore chlorophyll fluorescence, was dependent primarily on the supply of CO_2 through the stomata on the upper surface.

We used both F' and $1 - F'/F_m'$ images to quantify fluorescence heterogeneity in this study. (We inverted the greyscales of the $1 - F'/F_m'$ images so that they would be visually more comparable with the thermal images.) The quantity $1 - F'/F_m'$ has been shown to be proportional to the quantum yield of PSII (Genty, Briantais & Baker 1989), and several previous studies on fluorescence heterogeneity have used images calculated from this quantity (Genty & Meyer 1994; Meyer & Genty 1998). However, the use of a high-PFD flash to create the F_m' image creates limitations in the acquisition and interpretation of fluorescence data. First, the frequency with which F_m' images can be safely captured is limited because of potential effects of the high-PFD flash on the photosynthetic machinery (Maxwell & Johnson 2000). For many studies this is not a problem, but in this study we were interested in acquiring detailed time courses for fluorescence images, and it was important to sample frequently enough that aspects of the dynamics were not missed. Second, although sufficiently infrequent high-PFD flashes may have little effect on the photosynthetic machinery, their effects on stomatal conductance are less clear. It is possible that the dynamics of fluorescence heterogeneity observed in this study and others were caused by or reinforced by the regularly spaced high-PFD flashes.

Examination of images from experiments with both F' and $1 - F'/F_m'$ images revealed that complex temporal and spatial fluorescence patterns were present in experiments with or without F_m' images, and that most of the fluorescence heterogeneity in the $1 - F'/F_m'$ images was present in the F' images (see Fig. 3). In addition, there were no rapid changes in fluorescence time series or time lapse movies that were obvious in the F' images that were not evident in the $1 - F'/F_m'$ images. Although we have no way of unequivocally determining if the fluorescence patterns in the absence of the flashes were exactly the same as would have occurred in the presence of flashes, comparison of data from the two types of experiments revealed no obvious differences. We conclude that the existence of the fluorescence patterns was not the result of regular flashes of light necessary to capture time sequences of $1 - F'/F_m'$ images. We also conclude from these experiments that $1 - F'/F_m'$ images, when taken at 3 min intervals, captured most of the temporal dynamics in the fluorescence patches.

Interpretation of fluorescence images in terms of stomatal conductance requires several assumptions. If oxygen concentrations are kept low, the quantum efficiency of photosystem II (Φ_{PSII}), which can be determined from fluorescence measurements (Genty *et al*. 1989; Genty & Meyer 1994), reflects primarily electron transport to CO_2. If PFD and such processes as electron flow through the Mehler reaction or towards nitrate reduction are constant, the quantum yield of photosystem II is uniquely related to the rate of CO_2 fixation. It can then be argued that the primary determinant of CO_2 fixation rate is CO_2 supply through the stomata, and therefore heterogeneity in fluorescence should reflect heterogeneity in stomatal conductance. Similarly, non-photochemical fluorescence quenching processes are induced at low values of c_i, and the degree of non-photochemical quenching can also be approximated using fluorescence images (Daley *et al*. 1989; Cardon *et al*. 1994).

Thus, interpretation of either Φ_{PSII} images or images of non-photochemical quenching in terms of stomatal conductance relies on the assumption that there are no intrinsic changes in the photosynthetic machinery. Several studies have called this assumption into question, however. Heterogeneity in $^{14}CO_2$ assimilation (Wise *et al*. 1992) and in chlorophyll fluorescence (Osmond, Kramer & Luttge 1999), produced by severe water stress, could not be relieved by high CO_2, suggesting that changes in mesophyll capacity for photosynthesis were responsible for some of the non-uniformities. Similarly, heterogeneity in chlorophyll fluorescence during photosynthetic induction (Bro, Meyer & Genty 1996) and in response to ABA (Meyer & Genty 1999) has been shown to be partly metabolic in origin. These results raise the question of whether the complex patterns of chlorophyll fluorescence that we observed were really caused by patterns of stomatal conductance or whether heterogeneity in other metabolic parameters might be at least partially responsible.

To address this question we imaged chlorophyll fluorescence and leaf temperature simultaneously. We could detect no cross-sensitivity between the fluorescence and thermal cameras (Figs 1 & 2). Visualization of conductance patterns for only the upper surface with thermography was accomplished by maintaining a small Δw for the lower surface while increasing the Δw for the upper surface. Although it is unlikely that conductance patches formed on the lower surface in these experiments because there was no change in the gas-exchange measurements for that surface, any patches that might have formed on the lower surface would have had only a minimal effect on leaf temperature because Δw for the lower surface was small (a low Δw reduces the effect of stomatal conductance on transpiration and therefore on leaf temperature). These consider-

ations make it likely that the patterns recorded by the thermal camera were primarily the result of stomatal conductance patterns for the upper surface.

In comparing the thermal and fluorescence images shown in Figs 3 and 6, and the pixel intensity time series shown in Figs 4 and 5, it is important to recognize that even if all changes in fluorescence leaf temperature were caused by stomatal conductance, the two sets of images would not be identical because neither technique provides an exact map of stomatal conductance. For example, even for stomatal patches with 'sharp' edges (i.e an abrupt transition from wide open to closed stomata), both fluorescence and thermal images would show blurred edges. The fluorescence images will be blurred by lateral CO_2 diffusion within the leaf, which will depend on the internal anatomy of the mesophyll. Similarly, the edges of the patches in the thermal images will be blurred as heat flows from the warmer to the cooler portions of the leaf (Jones 1999). In addition, the pixel resolution of the thermal camera was considerably less than that of the fluorescence camera, and this made direct comparison of pixel intensities for a given region of the images impossible. Because of this, the 2.3 mm × 2.3 mm regions of comparison (Figs 4 & 5) contained different numbers of pixels and were not exactly the same size.

Despite these inherent limitations, the thermal and fluorescence patterns in this study were remarkably similar both visually and statistically, and we were unable to detect any consistent differences between the two sets of images. These data therefore suggest that the dynamic patterns in chlorophyll fluorescence observed in this study were caused primarily by patterns in stomatal conductance. It remains possible that subtle changes in chlorophyll fluorescence were caused by other factors, as has been suggested by other studies (Wise *et al*. 1992; Bro *et al*. 1996; Meyer & Genty 1999; Osmond *et al*. 1999), but the dynamics and overall patterns of stomatal conductance appear resolvable with chlorophyll fluorescence images.

In summary, we acquired fluorescence and thermal images of stomatal patchiness for a single surface of a leaf at sufficiently short time intervals to unambiguously track the dynamics of the patches. These experiments revealed the presence of stomatal conductance patches that appeared to move coherently across the leaf surface. These patches resemble in many ways a self-propagating solitary wave, or 'soliton'. In many cases, these solitons moved through specific regions of the leaf repeatedly and at regular intervals. This appeared as oscillatory behaviour when these regions were viewed in isolation (Figs 4 & 5). Although we are not suggesting that all oscillatory behaviour in stomata can be attributed to this phenomenon, the repeated movement of these solitons caused at least some of the apparent oscillatory behaviour in our experiments. The presence of these coherent, moving patches places constraints on the mechanisms that can be considered for the formation of patches. In addition, computer simulations of locally connected networks show that the presence of coherent propagating structures can be associated with some forms of emergent behaviour, including computation (Crutchfield & Mitchell 1995). The presence of these structures in stomatal dynamics may have important ramifications for the interpretation of stomatal behaviour in intact leaves (Peak *et al*. 2004).

ACKNOWLEDGMENTS

We thank Rand Hooper for technical assistance.

REFERENCES

Beyschlag W. & Eckstein J. (1998) Stomatal patchiness. In *Progress in Botany* (eds K. Behnke, K. Esser, J.W. Kadereit, U. Luttge & M. Runge), pp. 283–298. Springer-Verlag, Berlin, Germany.

Beyschlag W. & Pfanz H. (1992) A fast method to detect the occurrence of nonhomogenous distribution of stomatal aperture in heterobaric plant leaves. Experiments with *Arbutus unedo* L. during the diurnal course. *Oecologia* **82,** 52–55.

Bro E., Meyer S. & Genty B. (1996) Heterogeneity of leaf CO_2 assimilation during photosynthetic induction. *Plant, Cell and Environment* **19,** 1349–1358.

Buckley T.N., Farquhar G.D. & Mott K.A. (1997) Qualitative effects of patchy stomatal conductance distribution features on gas exchange calculations. *Plant, Cell and Environment* **20,** 867–880.

Buckley T.N., Farquhar G.D. & Mott K.A. (1999) Carbon-water balance and patchy stomatal conductance. *Oecologia* **118,** 132–143.

Cardon Z.G., Mott K.A. & Berry J.A. (1994) Dynamics of patchy stomatal movements, and their contirbution to steady-state and oscillating stomatal conductance calculated with gas-exchange techniques. *Plant, Cell and Environment* **17,** 995–1008.

Crutchfield J.P. & Mitchell M. (1995) The evolution of emergent computation. *Proceedings of the National Academy of Sciences of the USA* **92,** 10742–10746.

Daley P.F., Raschke K., Ball J.T. & Berry J.A. (1989) Topography of photosynthetic activity of leaves obtained from video images of chlorophyll fluorescence. *Plant Physiology* **90,** 1233–1238.

Genty B. & Meyer S. (1994) Quantitative mapping of leaf photosynthesis using chlorophyll fluorescence imaging. *Australian Journal of Plant Physiology* **22,** 277–284.

Genty B., Briantais J.-M. & Baker N.R. (1989) The relationship between the quantum yield of photosynthetic electron transport and quenching of chlorophyll fluorescence. *Biochimica et Biophysica Acta* **990,** 87–92.

Haefner J.W., Buckley T.N. & Mott K.A. (1997) A spatially explicit model of patchy stomatal responses to humidity. *Plant, Cell and Environment* **20,** 1087–1097.

Jones H.G. (1999) Use of thermography for quantitative studies of spatial and temporal variation of stomatal conductance over leaf surfaces. *Plant, Cell and Environment* **22,** 1043–1055.

Maxwell K. & Johnson G.N. (2000) Chlorophyll fluorescence – a practical guide. *Journal of Experimental Botany* **51,** 658–668.

Meyer S. & Genty B. (1998) Mapping intercellular CO_2 mole fraction (Ci) in *Rosa rubiginosa*leaves fed with abscisic acid by using chlorophyll fluorescence imaging – Significance of Ci estimated from leaf gas exchange. *Plant Physiology* **116,** 947–957.

Meyer S. & Genty B. (1999) Heterogeneous inhibition of photosynthesis over the leaf surface of *Rosa rubiginosa* L. during water stress and abscisic acid treatment: induction of a metabolic component by limitation of CO_2 diffusion. *Planta* **210,** 126–131.

Mott K.A. (1988) Do stomata respond to CO_2 concentrations other than intercellular? *Plant Physiology* **86,** 200–203.

Mott K.A. & Buckley T.N. (1998) Stomatal heterogeneity. *Journal of Experimental Botany* **49,** 407–417.

Mott K.A. & Buckley T.N. (2000) Patchy stomatal conductance: emergent collective behaviour of stomata. *Trends in Plant Science* **5,** 258–262.

Mott K.A. & Franks P.J. (2001) The role of epidermal turgor in stomatal interactions following a local perturbation in humidity. *Plant, Cell and Environment* **24,** 657–662.

Mott K.A. & O'Leary J.W. (1983) Stomatal behavior and CO_2 exchange characteristics in amphistomatous leaves. *Plant Physiology* **74,** 47–51.

Mott K.A., Cardon Z.G. & Berry J.A. (1993) Asymmetric patchy stomatal closure for the two surfaces of *Xanthium strumarium* L. leaves at low humiditiy. *Plant, Cell and Environment* **16,** 25–34.

Mott K.A., Denne F. & Powell J. (1997) Interactions among stomata in response to perturbations in humidity. *Plant, Cell and Environment* **20,** 1098–1107.

Mott K.A., Shope J.C. & Buckley T.N. (1999) Effects of humidity on light-induced stomatal opening: evidence for hydraulic coupling among stomata. *Journal of Experimental Botany* **50,** 1207–1213.

Osmond C.B., Kramer D. & Luttge U. (1999) Reversible, water stress-induced non-uniform chlorophyll fluorescence quenching in wilting leaves of *Potentilla reptans* may not be due to patchy stomatal responses. *Plant Biology* **1,** 618–624.

Parkhurst D.F. & Mott K.A. (1990) Intercelluar diffusion limits to CO_2 uptake in leaves. Studies in air and helox. *Plant Physiology* **94,** 1024–1032.

Parkhurst D.F., Wong S.C., Farquhar G.D. & Cowan I.R. (1986) Gradients of intercellular CO_2 levels across the leaf mesophyll. *Plant Physiology* **86,** 1032–1037.

Peak D., West J.D., Messinger S. & Mott K.A. (2004) Evidence for complex, collective dynamics and emergent, distributed computation in plants. *Proceedings of the National Academy of Sciences of the USA* **101,** 918–922.

Siebke K. & Weis E. (1995) 'Assimilation images' of leaves of *Glechoma hederacea;* analysis of non-synchronous stomata related oscillations. *Planta* **196,** 155–165.

Terashima I. (1992) Anatomy of non-uniform leaf photosynthesis. *Photosynthesis Research* **31,** 195–212.

Terashima I., Wong S.-C., Osmond C.B. & Farquhar G.D. (1988) Characterisation of non-uniform photosynthesis induced by abscisic acid in leaves having different mesophyll anatomies. *Plant Cell Physiology* **29,** 385–394.

Wise R.R., Ortiz-Lopez A. & Ort D.R. (1992) Spatial distribution of photosynthesis during drought in field-grown and acclimated and nonacclimated growth chamber-grown cotton. *Plant Physiology* **100,** 26–32.

Received 26 April 2004; received in revised form 28 September 2004; accepted for publication 19 November 2004